Human Molecular Genetics, 2007, Vol. 16, No. 21 ***2529–2541***
doi:10.1093/hmg/ddm145
Advance Access published on June 21, 2007

Regional rearrangements in chromosome 15q21 cause formation of cryptic promoters for the *CYP19* (aromatase) gene

Masashi Demura[1,†], Regina M. Martin[1,2,†], Makio Shozu[3], Siby Sebastian[4], Kazuto Takayama[5], Wei-Tong Hsu[6], Roger A. Schultz[7], Kirk Neely[8], Michael Bryant[9], Berenice B. Mendonca[2], Keiichi Hanaki[10], Susumu Kanzaki[10], David B. Rhoads[11], Madhusmita Misra[11] and Serdar E. Bulun[1,*]

[1]Division of Reproductive Biology Research, Northwestern University Feinberg School of Medicine, Chicago, IL 60611, USA, [2]Unidade de Endocrinologia do Desenvolvimento, Laboratorio de Hormonios e Genetica Molecular LIM/42, Divisao de Endocrinologia, Hospital das Clinicas, Faculdade de Medicina, Universidade de Sao Paulo, Sao Paulo 01065-970, Brazil, [3]Department of Obstetrics and Gynecology, Graduate School of Medicine, Chiba University, Chiba 260-8670, Japan, [4]Department of Pathology, Duke University Medical Center, Durham, NC 27710, USA, [5]Department of Obstetrics and Gynecology, Tohoku University School of Medicine, Sendai 980-8574, Japan, [6]Department of Pediatrics, Rush Medical School, Chicago, IL 60612, USA, [7]Department of Pathology, University of Texas Southwestern Medical Center at Dallas, Dallas, TX 75390, USA, [8]Department of Pediatrics, Stanford University, Palo Alto, CA 94305, USA, [9]Department of Pediatrics, Children's Hospital, Los Angeles, CA 90027, USA, [10]Division of Pediatrics and Perinatology, Tottori University, Yonago, Japan and [11]Pediatric Endocrine Unit, Mass General Hospital for Children and Harvard Medical School, Boston, MA 02114, USA

Received March 29, 2007; Revised June 1, 2007; Accepted June 5, 2007

Production of appropriate quantities of estrogen in various tissues is essential for human physiology. A single gene (*CYP19*), regulated via tissue-specific promoters, encodes the enzyme aromatase, which catalyzes the key step in estrogen biosynthesis. Aromatase excess syndrome is inherited as autosomal dominant and characterized by high systemic estrogen levels, short stature, prepubertal gynecomastia and testicular failure in males, and premature breast development and uterine pathology in females. The underlying genetic mechanism is poorly understood. Here, we characterize five distinct heterozygous rearrangements responsible for aromatase excess syndrome in three unrelated families and two individuals (nine patients). The constitutively active promoter of one of five ubiquitously expressed genes located within the 11.2 Mb region telomeric to the *CYP19* gene in chromosome 15q21 cryptically upregulated aromatase expression in several tissues. Four distinct inversions reversed the transcriptional direction of the promoter of a gene (CGNL1, TMOD3, MAPK6 or TLN2), placing it upstream of the CYP19 coding region in the opposite strand, whereas a deletion moved the promoter of a fifth gene (*DMXL2*), normally transcribed from the same strand, closer to *CYP19*. The proximal breakpoints of inversions were located 17–185 kb upstream of the CYP19 coding region. Sequences at the breakpoints suggested that the inversions were caused by intrachromosomal nonhomologous recombination. Splicing the untranslated exon downstream of each promoter onto the identical junction upstream of the translation initiation site created CYP19 mRNA encoding functional aromatase protein. Taken together, small rearrangements may create cryptic promoters that direct inappropriate transcription of CYP19 or other critical genes.

*To whom correspondence should be addressed at: Division of Reproductive Biology Research, Northwestern University Feinberg School of Medicine, 303 E. Superior Street, Suite 4-123, Chicago, IL 60611 USA. Tel: +1 3125030520; Fax: +1 3125030095; Email: s-bulun@northwestern.edu
†The authors wish it to be known that, in their opinion, the first two authors should be regarded as joint First Authors.

INTRODUCTION

Aromatase catalyzes the final step of estrogen biosynthesis, the conversion of C_{19} steroids to estrogens. A single gene (*CYP19*) encodes aromatase, and is expressed in specific tissues, including the brain, gonads, fat, skin and the placenta (1). The entire *CYP19* gene spans ~123 kb and is transcribed from the telomere to the centromere (1–3). The 30 kb 3′ end of this gene contains nine exons (II–X), which encode the aromatase protein. The ATG translation initiation site is located 38 bp downstream of a common splice acceptor site in coding exon II. The 93 kb 5′ flanking region of the gene contains a number of 'physiological' promoters with 5′ untranslated first exons that are controlled in a tissue-specific manner. These untranslated exons are spliced alternatively onto a common splice junction, leading to promoter-specific mRNA species that encode the identical aromatase protein (1).

The farthest upstream promoter is I.1, and its activity causes splicing of exon I.1 onto the common splice acceptor site that is 93 kb downstream. The most proximal gonad-specific promoter II and the other two proximal promoters, I.3 (expressed in adipose tissue and breast cancer) and I.6 (expressed in bone) are located within the 1 kb region upstream of the common splice junction. The promoters specific for the brain (I.f) and skin (I.4) are localized at ~33 and ~73 kb upstream of the common splice junction, respectively (1,4). In adipose tissue or cultured adipose fibroblasts from breast, abdomen, buttocks and thighs, promoters I.4 (major) and I.3/II (minor) are used (4). Untreated skin fibroblasts in culture use promoter I.4 (5).

In normal men, estrogen arises primarily from aromatization of steroid precursors in extra-gonadal tissues (6). Excessive estrogen formation in boys causes pre- and/or peripubertal gynecomastia and premature growth with early fusion of epiphyses, resulting in short stature. Overproduction of estrogen by testicular Sertoli tumors may cause prepubertal gynecomastia, which can present as an isolated abnormality or in connection with Peutz–Jeghers syndrome (7–13). Estrogen-secreting Leydig cell tumors also can induce gynecomastia (14). Feminizing adrenocortical and hCG-producing tumors are extremely rare causes of prepubertal gynecomastia (15,16). It has been suggested that hereditary gynecomastia might also develop as a result of late-onset 17-ketosteroid reductase deficiency (17). Increased conversion of steroid precursors to estrogens in extraglandular tissues represents another cause of estrogen excess. Hemsell *et al*. (18) described the first case of feminized, prepubertal, adopted boy in whom large amounts of estrone and estradiol were produced by extraglandular aromatization of plasma androstendione. This was followed by a number of case reports, in which this disorder was referred to as 'aromatase excess syndrome' (18). It affects both sexes and is manifest as short stature and prepubertal gynecomastia or premature thelarche or irregular uterine bleeding (19).

In a previous case report, constitutively active promoters of two genes located proximally to the CYP19 coding region were postulated to cryptically stimulate CYP19 transcription, leading to aromatase excess syndrome (20). The underlying genetic mechanism, however, remained unknown to date. Here, we describe the cloning and mechanisms of five distinct heterozygous rearrangements affecting the *CYP19* gene in chromosome 15q21, which are responsible for aromatase excess syndrome in three unrelated families and two individuals (nine patients).

RESULTS

Aromatase enzyme activity and mRNA levels in tissues of affected patients

We examined three families and two sporadic cases with aromatase excess syndrome. Aromatase activity and mRNA levels in lymphoblastoid cell lines (LCLs) from seven affected patients correlated closely (Fig. 1). Enzyme activity and aromatase mRNA levels were significantly higher in members of families 1 and 2, the affected daughter in family 2 and in sporadic case 1 than those of controls (Fig. 1). Compared with control subjects, aromatase activity and mRNA levels in LCLs were not elevated in members of family 3 and in sporadic case 2. Aromatase activity and mRNA levels in skin fibroblasts of sporadic case 2 were 11 and 32 times higher than those in control subjects, respectively (data not shown). Aromatase activity and mRNA levels were previously reported as elevated in cultured skin fibroblasts of a member of family 3 (21).

Determination of 5′ UTRs of CYP19 mRNA and mapping to the human genome

We have reported CGNL1 and TMOD3 as cryptic promoters in family 1 and sporadic case 1, respectively (20). The 5′ RACE of the CYP19 mRNA from skin fibroblasts revealed novel 5′ UTRs in the affected patients, but not in the controls (data not shown). Mapping of these novel sequences to the human genome showed that they normally comprise the first exons of two neighboring genes: *MAPK6* in family 2 and *DMXL2* in family 3. Two distinct unknown sequences detected as novel 5′ UTRs in sporadic case 2 were located 40 kb apart from each other and mapped to 11.2 Mb upstream of the first coding exon (exon II) of the *CYP19* gene. The 3′ RACE was used to characterize these sequences as novel, alternative, untranslated exons of the *TLN2* gene. This was confirmed by reverse transcriptase-polymerase chain reaction (RT-PCR) analysis of TLN2 mRNA in normal skin fibroblasts (data not shown). All abnormal 5′ UTRs were mapped within the 11.2 Mb region telomeric to the *CYP19* gene in chromosome 15q21 (Table 1). According to the genome database (www.ncbi.nlm.nih.gov/mapview), the *CGNL1*, *TMOD3*, *MAPK6* and *TLN2* genes are transcribed from the same DNA strand in the telomeric direction opposite to that of *CYP19*. Thus, we postulated that inversion mutations caused the promoters of these four genes to lie upstream of the *CYP19* gene and act cryptically to regulate its expression. In contrast, the *DMXL2* gene is transcribed from the same strand as the *CYP19* gene in the centromeric direction and is located at 380 kb 5′ upstream of the *CYP19* gene. This led us to postulate that a deletion mutation moved the DMXL2 promoter closer to the coding region of CYP19 in order to cryptically regulate its expression. Moreover, a potential deletion mutation would suggest the presence of at least one *cis*-regulatory element that would normally prevent the

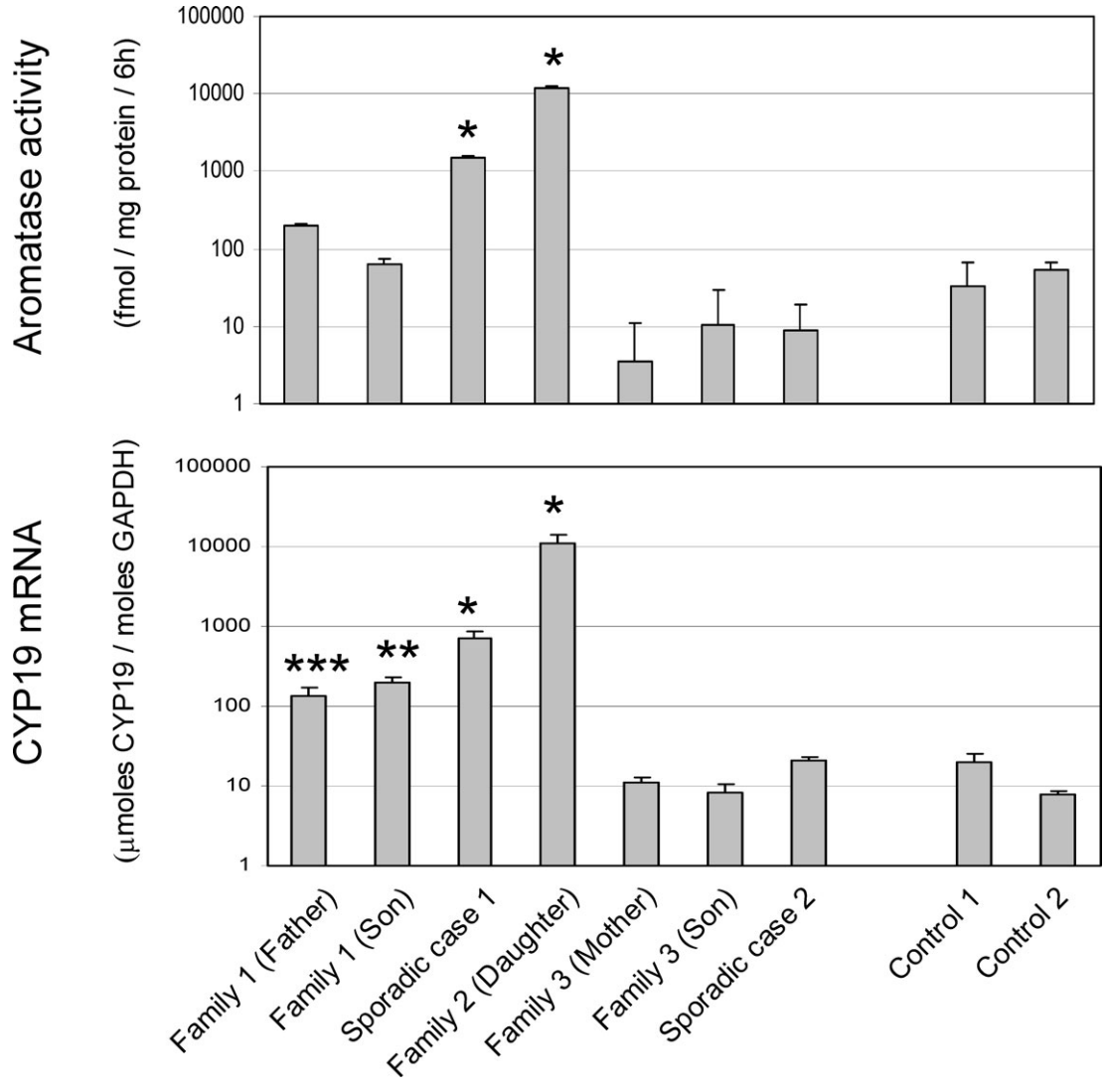

Figure 1. Aromatase activity and CYP19 mRNA levels in LCLs. Aromatase activity in LCLs from sporadic case 1 and the daughter in family 2 differed significantly from that of controls. CYP19 mRNA levels in LCLs from the father and his son in family 1, sporadic case 1 and the daughter in family 2 were significantly higher compared with those in LCLs from control subjects. $^{*}P < 0.0001$, $^{**}P < 0.002$, $^{***}P < 0.01$, two-tailed Student's *t*-test.

DMXL2 promoter from affecting the CYP19 coding region. To confirm our hypotheses, we cloned the breakpoints of four inversions and demonstrated by PCR a complex deletion mutation in the fifth case (family 3).

Cloning the breakpoints of four inversions

Family 1 We designed a series of primer pairs that would amplify overlapping <20 kb segments and postulated that a chimeric PCR product, comprised of sequences in the first introns of *CYP19* and *CGNL1* genes, would be amplified only from the affected patients, since these two genes normally lie 6.1 Mb apart. Following this strategy, we obtained a ~6 kb PCR product using primers 1F and 1R only from affected members of family 1, but not from unaffected family members (data not shown) (Fig. 2A; Table 2). Sequencing of this product or one of its amplified portions (1033 bp)

Table 1. Cryptic promoters in chromosome 15q21

Case	Gene normally regulated by the cryptic promoter	Strand location	Distance from the translation start site of the CYP19 gene (Mb)
Family 1[a]	*CGNL1*	+	~6.1
Sporadic case 1[a]	*TMOD3*	+	~0.59
Family 2	*MAPK6*	+	~0.75
Family 3	*DMXL2*	−	~0.38
Sporadic case 2	*TLN2*	+	~11.2

Using rapid amplification of 5′ cDNA ends, we identified five abnormal 5′ untranslated regions (UTRs) in CYP19 (aromatase) mRNA from three families and two sporadic patients affected by aromatase excess syndrome. All five genes mapped to chromosome 15q21. The definition of the strand location is based on the MapViewer Web site. The CYP19 gene is located on the minus strand.
[a]These 5′ UTRs were reported previously (20).

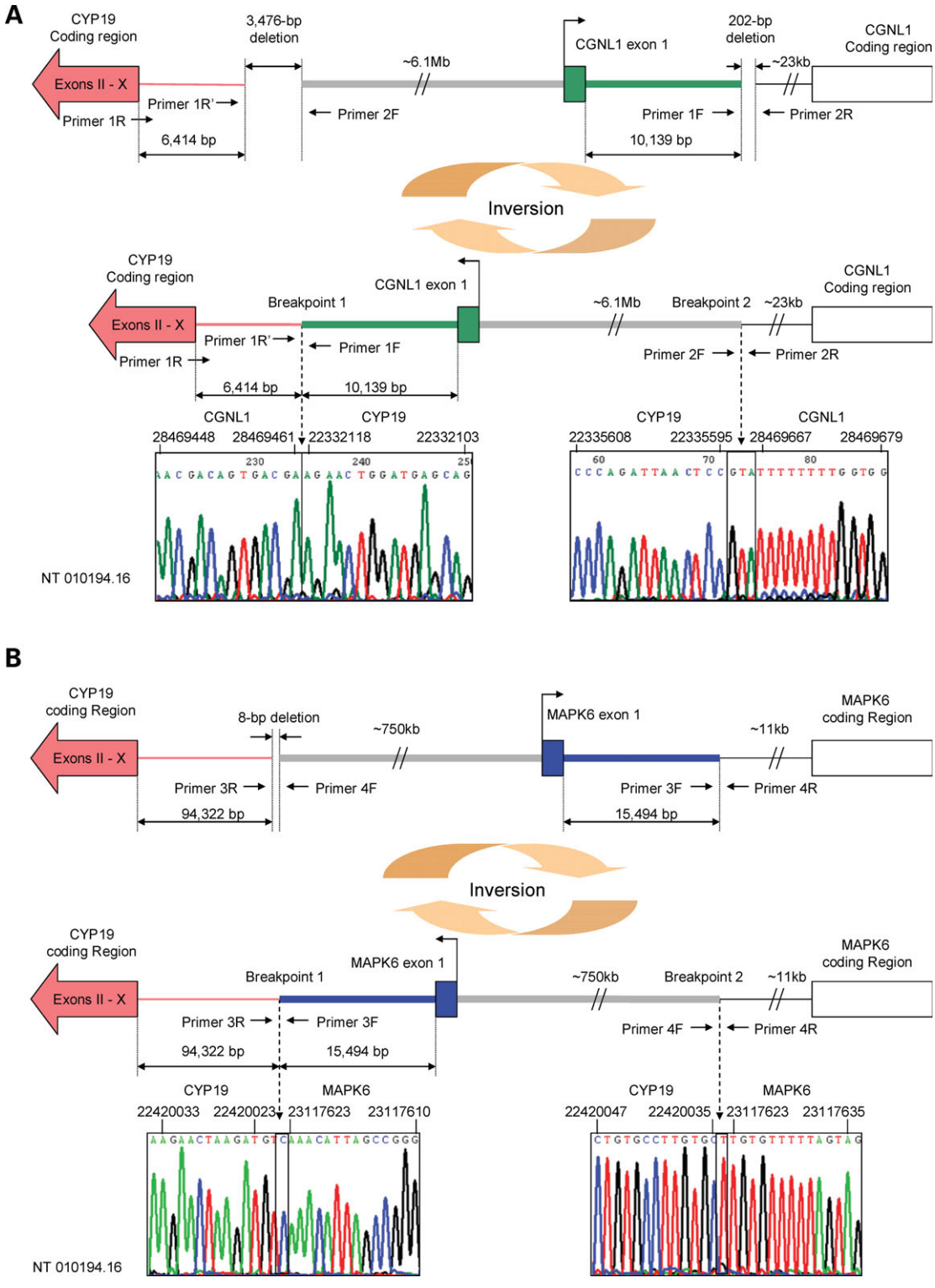

Figure 2. Depiction of rearrangements in chromosome 15q21 and pedigrees. (**A**) CGNL1/CYP19 rearrangement in family 1. The inversion mutation moved the CGNL1 promoter and first exon ~16.5 kb upstream of the CYP19 exon II. We found that a 3476 bp region at the CYP19 and a 202 bp region at the CGNL1 sides were deleted, and that the 6.1 Mb intervening segment was inverted. (**B**) MAPK6/CYP19 rearrangement in family 2. A ~750 kb segment was inverted, giving rise to fusion of the MAPK6 promoter regulatory region ~110 kb upstream of the CYP19 coding region. In this instance, there was a very small (8 bp) deletion at the CYP19 side and no deletion at the MAPK6 side. (**C**) TLN2/CYP19 rearrangement in sporadic case 2. We found that inversion of a ~11.2 Mb segment moved the promoter and first 2 exons of the TLN2 gene ~185 kb upstream of the CYP19 coding region. Small (1 and 8 bp) deletions were found at both sides of the breakpoint. (**D**) TMOD3/CYP19 rearrangement in sporadic case 1. The breakpoint involved the inversion of a ~590 kb segment giving rise to the fusion of the TMOD3 promoter region ~176 kb upstream of the CYP19 coding region. Nucleotide numbers correspond to the Contig NT_010194.16. Overlapped sequences common to both sequences are boxed. Inserted sequences were boxed with dotted line.

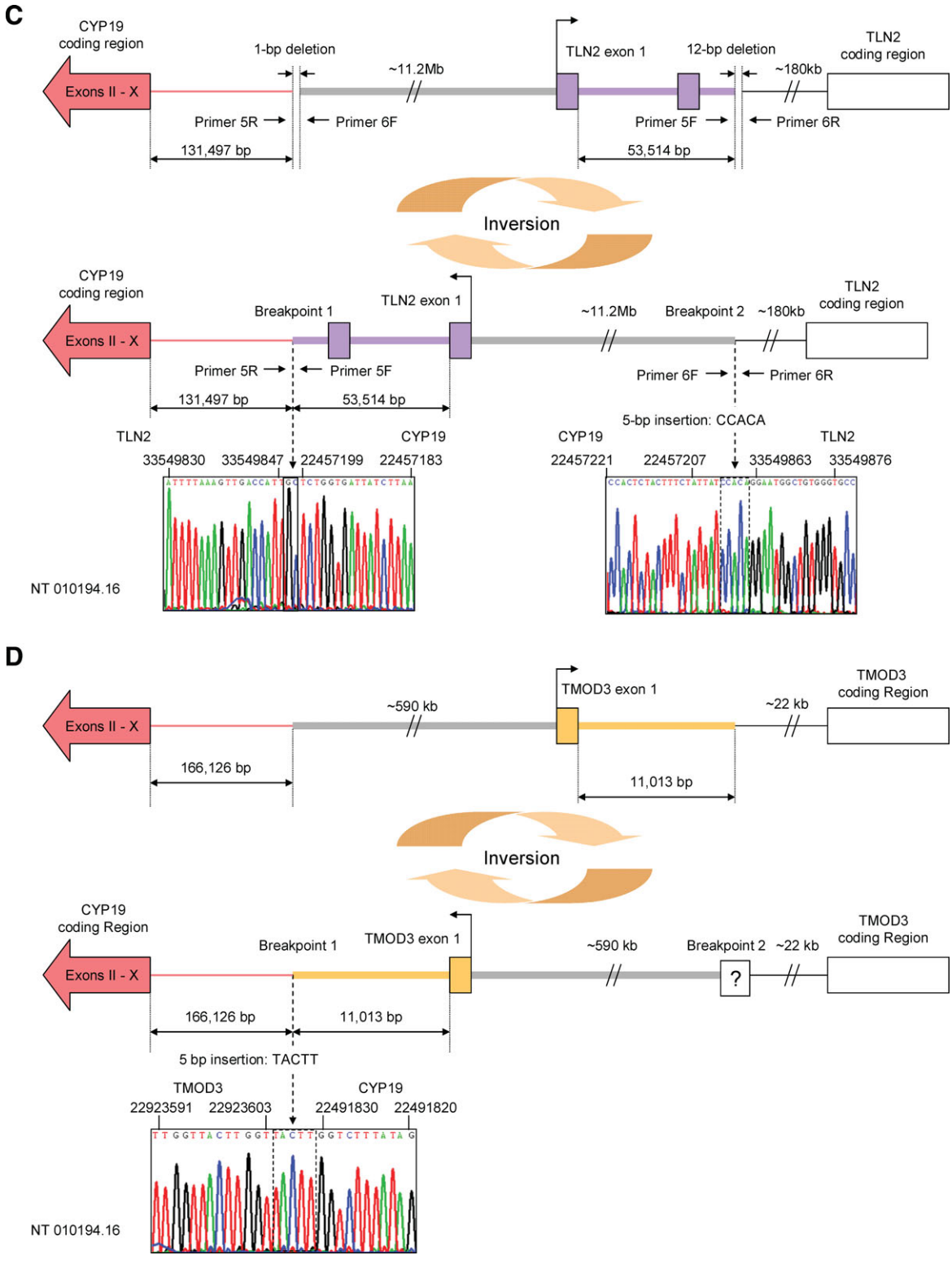

Figure 2. Continued.

using nested primers (primers 1F and 1R′) revealed the first breakpoint (Figs. 2A and 3A; Table 2). On the basis of the sequence of the first breakpoint, new primers (primers 2F and 2R) were designed to clone the second breakpoint (Fig. 2A), which was found in a 172 bp PCR product (data not shown).

Table 2. Primers used in this study

Name	Sequence (5′–3′)	Position[a]	AT	Size
Primer 1F	ACTAAAATGGTTGGGGCTCAACAAAGAA	28469202–28469229	68	
Primer 1R	AGAGTCTCAGGTTCCTTTAGACGCTTGG	22325918–22325945		
Primer 1R′	TCAAATTCTTCCCTCTGTTTCCTCTCCT	22331319–22331346		
Primer 2F	TTGTGCAATCTGTCTTCCCCAGATTAAC	22335598–22335625		
Primer 2R	TCAGGGGGATGAAAAAGTTTTGGAATTA	28469777–28469804		
Primer 3F	GCCCTGGCGAAGAGTTGTTCTTTCTCTT	23117352–23117379		
Primer 3R	GCCATGGTATTCAGACGAGAACCCAAGT	22419812–22419839		
Primer 4F	TATGCACCTGGGCTTTGGAATCAGACCT	22420281–22420308		
Primer 4R	TATGAAGAGATAACAAGGCCAGGCGCAG	23117744–23117771		
Primer 5F	TTTAATTTTTGCAAATGGCTGTGAATGG	33549629–33549656		
Primer 5R	CCCAGGACAATGACCTCTAAGGACTCTT	22456544–22456571		
Primer 6F	GGTAGGCCAAGGTGGGAAGATTGATTT	22457716–22457742		
Primer 6R	GCAACCTCTACCTCTTGGCGATTCTC	33550356–33550381		
Primer 7F	TAGCCAAAATGATGTGGGAAATATCGAC	22923447–22923474		
Primer 7R	CATACGTGTGCTTATTCACATGGTGTCC	22491743–22491770		
Exon II F	TACAGCACCCTCTGAAGCAA	22325768–22325787	68	144
Exon II R	GGGTTCAGCATTTCCAAAAC	22325644–22325663		
Exon II Probe	FAM-TGCCCCCTCTGAGGTCAAGGA-TAMRA	22325674–22325694		
Segment A F	AGTGAGGGGCAAAATTGGTA	22335322–22335341		103
Segment A R	GGAGATTCCATGAGCCTTGA	22335405–22335424		
Probe A	FAM-CCCATCTGTGGGCCCTCAGA-TAMRA	22335351–22335370		
Segment B F	GGACCAGACCTGTGTCCACT	22375620–22375639		135
Segment B R	GGGGGTCCTGCCTATACATT	22375505–22375524		
Probe B	FAM-CCCCGACCTTCCCCCAGTGT-TAMRA	22375526–22375545		
Segment C F	ATAGGAGCAATTGGGGAGGT	22435762–22435781		139
Segment C R	CCCAAAATGAACTCCCTCCT	22435749–22435768		
Probe C	FAM-TGGCCTCTGGCTGCCTGACT-TAMRA	22435643–22435662		
Segment D F	CCACCTACTTGGCTTCAGGA	22490352–22490371		80
Segment D R	AACCTCAAAGCTAGGCCACA	22490292–22490311		
Probe D	FAM-CCTTATCAGCTGAAAGAAAATGCCTTGA-TAMRA	22490319–22490346		
Segment E F	CCCCAGCACTAGATCAGCTC	22525277–22525296		115
Segment E R	GCAGGCTTGCTTCTTGTGTT	22525182–22525201		
Probe E	FAM-ACCTAGGCACCAGGCCCGC-TAMRA	22525181–22525199		
Segment F F	GGCTTGAGCTTTTGTGTGCT	22590427–22590446		81
Segment F R	AGGAAAGAAAGCAGCAGCAG	22590366–22590385		
Probe F	FAM-AGCACCCCGCTTCCTTCCCT-TAMRA	22590406–22590425		
Segment G F	TCTTGGTACAGCCAAGTAACCA	22665226–22665245		87
Segment G R	TTCTGCTGTGATCTTTGCTCA	22665159–22665179		
Probe G	FAM-CAAAGCCCAGACAACCCTGCC-TAMRA	22665202–22665222		

F, forward primer; R, reverse primer; AT, annealing temperature.
[a]Primer and probe positions refer to numbering of the original sequence submission (Contig number NT_010194.16).

Family 2 The same PCR strategy was used to identify the breakpoints in the affected mother and her son and daughter but not the father or unaffected son (Figs. 2B and 3B). Primers 3F and 3R successfully amplified the first breakpoint only from the affected family members (Fig. 2B; Table 2). Primers 4F and 4R were used to amplify the second breakpoint (Fig. 2B; Table 2).

Sporadic case 1 PCR amplification of this patient's DNA did not readily reveal the breakpoints. Thus, we cloned each allele of this patient's DNA into separate BAC clones. One of the breakpoints was cloned by PCR in the BAC clone containing the mutated allele (Fig. 2D). This breakpoint was subsequently verified by PCR with primers 7F and 7R in the patient's DNA sample (Fig. 3D; Table 2). The second breakpoint remains to be elucidated. In this patient, the inversion of an estimated 590 kb segment gave rise to the fusion of the TMOD3 promoter region ~176 kb upstream of the CYP19 coding region.

Sporadic case 2 We cloned the breakpoints using primer pairs 5F/5R for the first breakpoint and 6F/6R for the second breakpoint (Fig. 2C; Table 2). The heterozygous rearrangement was found in the affected patient but not in a normal subject (Fig. 3C; Table 2).

Identification of a possible complex deletion by real-time PCR in family 3

The 5′ RACE demonstrated an abnormal chimeric *CYP19* mRNA comprised of exon I of the *DMXL2* gene and the coding exons II–X of the *CYP19* gene, suggesting that the DMXL2 promoter was utilized to transcribe the *CYP19* gene in the affected mother and her son, but not normal subjects. Since DMXL2 is located ~380 kb upstream (telomeric) of *CYP19* and transcribed from the same strand, we postulated that a deletion moved the DMXL2 promoter region closer upstream of the CYP19 exon II in one of the alleles (Fig. 3). We used real-time PCR to quantify seven segments of DNA

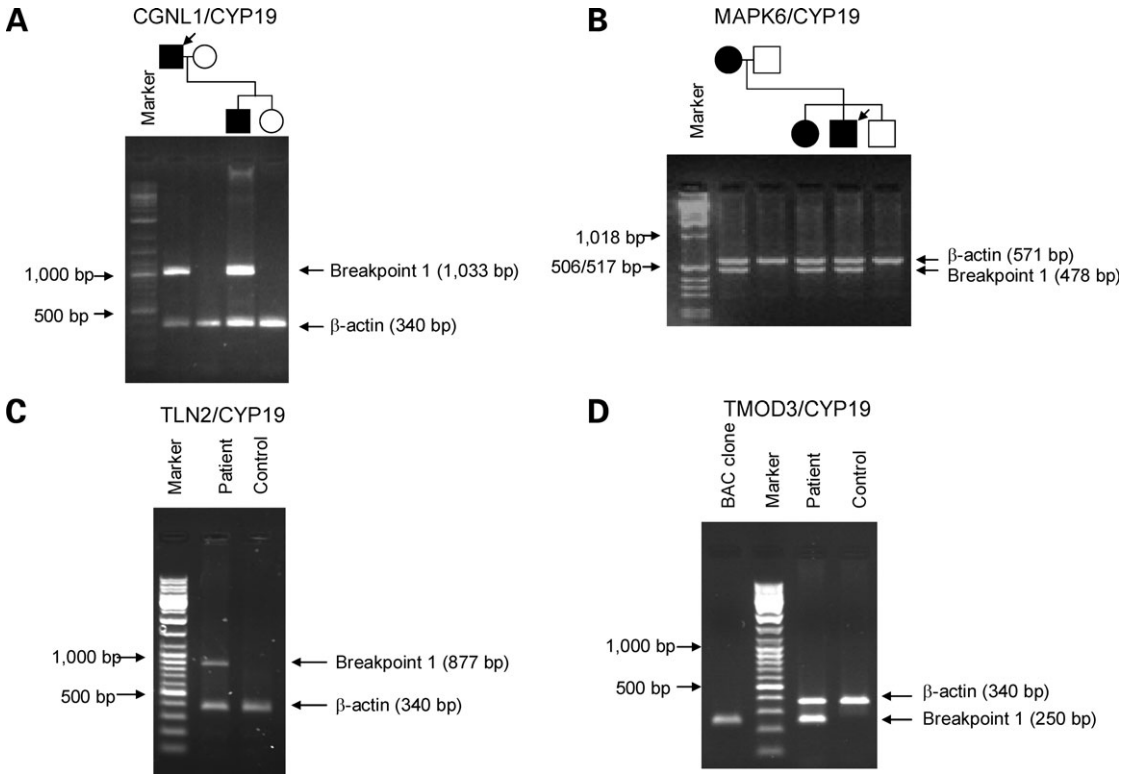

Figure 3. Screening of the mutation. (**A**) Family 1. The father and his son were heterozygous for this rearrangement, whereas DNA samples from the unaffected mother and daughter were negative. (**B**) Family 2. The abnormal PCR product was obtained only from the affected mother, son and daughter, but not the unaffected father and son. (**C**) Sporadic case 2. The abnormal PCR product was detected only from the patient and not in a normal control subject. (**D**) Sporadic case 1. The abnormal PCR product was detected from the BAC library and genomic DNA of the affected patient, but not in the normal control subject. Squares represent males, circles represent females, closed symbols indicate affected status, open symbols indicate unaffected status, arrowheads indicate probands.

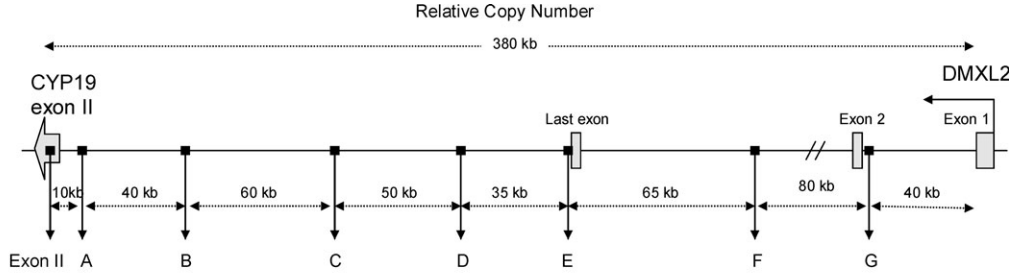

	A / Exon II	B / Exon II	C / Exon II	D / Exon II	E / Exon II	F / Exon II	G / Exon II
Son (family 3)	0.7 ± 0.4	0.4 ± 0.1	0.9 ± 0.1	0.8 ± 0.2	0.4 ± 0.1	0.2 ± 0.1	0.4 ± 0.2
Mother (family 3)	1.0 ± 0.4	0.4 ± 0.2	1.1 ± 0.5	0.8 ± 0.3	0.6 ± 0.3	0.4 ± 0.2	0.4 ± 0.2
Control (n=7)	1.0	1.0	1.0	1.0	1.0	1.0	1.0
Son (family 1)	0.4 ± 0.2						
Father (family 1)	0.4 ± 0.1						

Figure 4. Detection of deleted points by quantifying segments of DNA using real-time PCR in family 3. DNA samples from seven normal subjects were used as positive controls. The DNA amounts from the affected mother and her son were normalized to the average value from normal controls. As a positive control for deletion, we used DNA from the affected father and his son from family 1. Region A has been shown to be deleted in these patients (Fig. 2A).

that lie between CYP19 and DMXL2. The quantity of DNA in four of these regions was reduced by ∼60% compared with normal controls, indicating that at least a 145 kb segment from the second to last exon of DMXL2 and a <100 kb segment upstream of the *CYP19* gene were deleted in one of the alleles in the affected mother and her son but not in normal controls ($n = 7$, Fig. 4). Since markers flanking a 50 kb segment between these two heterozygous deletions existed at the same level as that seen in normal control subjects and the affected subjects, this appeared to be a complex rearrangement involving at least two deleted regions. A similar rearrangement was previously observed in patients with nephrogenic diabetes insipidus, who had a deletion of the *AVPR2* gene (22).

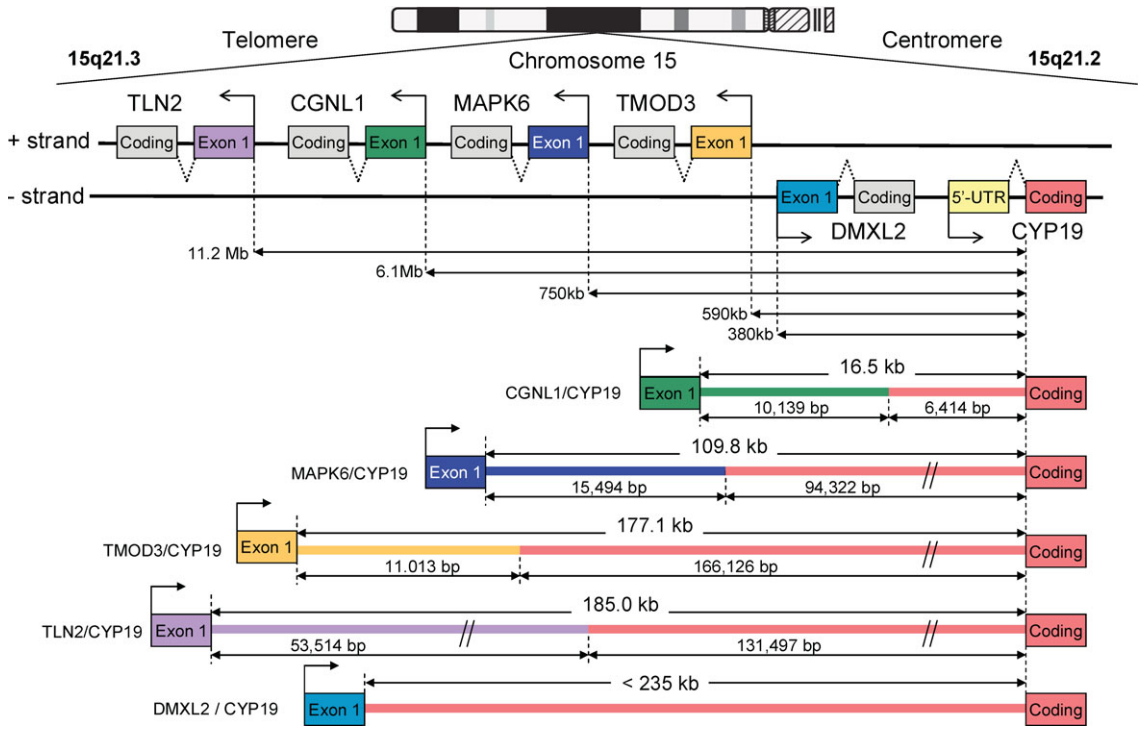

Figure 5. Summary of the five rearrangements identified in chromosome 15q21 from the three affected families and two sporadic cases.

Summary of mutations

Taken together, our data suggest that the constitutively active promoters of five ubiquitously expressed genes located within the 11.2 Mb region telomeric to the *CYP19* gene in chromosome 15q21 may direct cryptic upregulation of aromatase expression in patients with AES (Fig. 5). Four distinct inversions reversed the transcriptional direction of the promoters of four genes (*CGNL1*, *TMOD3*, *MAPK6* and *TLN2*), placing them upstream of the CYP19 coding region in the opposite strand, whereas a deletion moved the promoter of a fifth gene (*DMXL2*) closer to the *CYP19* gene. The proximal breakpoints varied in each case and were located 17–185 kb upstream of the CYP19 coding region.

Relative expression of genes whose promoters cryptically stimulate *CYP19* gene expression

The five genes whose promoters are believed to cryptically regulate the *CYP19* gene were found to be ubiquitously expressed in many human tissues, as determined by an analysis of cDNA libraries available on the Unigene website (www.ncbi.nlm.nih.gov/sites/entrez?db = unigene; Fig. 6). Thus, cryptic upregulation of the *CYP19* gene by the promoters of these five genes may account for nearly ubiquitous expression of aromatase, and thus accounting for the systemic, uncontrolled formation of estrogen in patients with AES (Fig. 6).

DISCUSSION

It has been suggested that the open chromatin conformation (euchromatin) is associated with areas of active transcription and may be more likely to undergo recombination, leading to cryptic regulation of other nearby genes (23). All five genes we identified whose promoters may cryptically stimulate *CYP19* gene expression are actively and ubiquitously transcribed as house-keeping genes. Thus, it is quite likely that the chromosome 15q21.2–3 region has an open chromatin conformation.

The breakpoints within chromosome 15q21 identified in this study were diverse with respect to both location and sequence. We considered three potential genetic mechanisms for the intrachromasomal rearrangements described in this report. One possibility was that the rearrangements were facilitated by the presence of region-specific low-copy repeats (LCRs) resulting from homologous recombination between paralogous genomic segments (24). Substrates for homologous recombination identified to date consist of significant lengths of sequence homology, LCRs that are usually ~10–400 kb with >97% identity (24). Direct LCRs are likely to lead to deletions or duplications, whereas inverted LCRs facilitate inversions. Therefore, we attempted to identify to LCRs within the 11.2 Mb region telomeric to the *CYP19* gene in chromosome 15q21. Only two copies of repeat fragments (~3 kb of 90% sequence identity) were found within this region. One was located 170 kb upstream of the CYP19 exon II, whereas the other was located within the DMXL2 intron I in an inverted orientation (data not shown). Thus, it seemed unlikely that the inversion mutations identified in present study occurred as a result of LCR-mediated homologous recombination.

Another possible cause for the rearrangements found in this study is the presence of repetitive elements, which comprise ~45% of the human genome (25,26). Short-interspersed nucleotide elements (SINEs) comprise 10% of the human

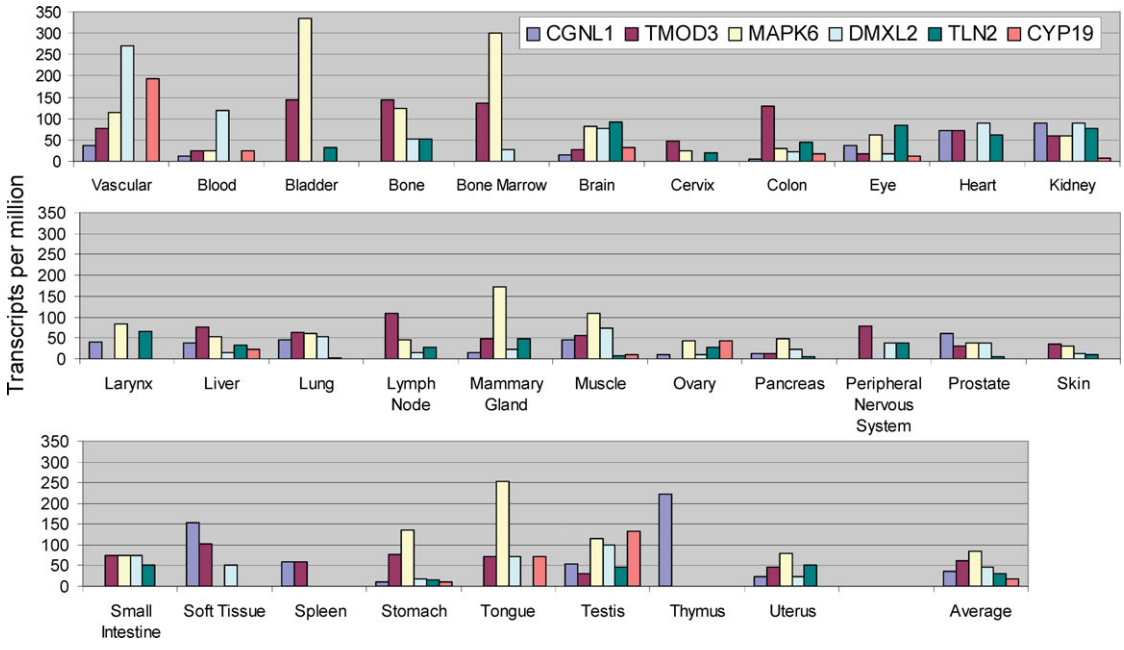

Figure 6. Expressed sequence tags profile. All five genes identified in this study were expressed ubiquitously in various human tissues, whereas CYP19 expression was primarily limited to the gonads, vascular tissue and the brain. Those data were obtained from the UniGene Web site (www.ncbi.nlm.nih.gov/sites/entrez?db = unigene).

Table 3. Interspersed repeats proximal to breakpoints

	Breakpoints	Breakpoints within repetitive elements	SINEs	LINEs	LTR elements	DNA elements	Total interspersed repeats (bp)
Family 1	CGNL1 side	Yes (SINE)	10 (1768 bp)	3 (512 bp)	1 (308 bp)	1 (220 bp)	2808
	CYP19 side	No	5 (925 bp)	6 (1194 bp)	0	0	2119
Family 2	MAPK6 side	Yes (SINE)	18 (4324 bp)	7 (1790 bp)	4 (1196 bp)	0	7310
	CYP19 side	No	4 (571 bp)	5 (1311 bp)	3 (1443 bp)	0	3325
Sporadic case 2	TLN2 side	No	5 (1350 bp)	1 (750 bp)	0	1 (224 bp)	2324
	CYP19 side	Yes (SINE)	9 (1623 bp	1 (177 bp)	2 (742 bp)	2 (1466 bp)	4008
Sporadic case 1	TMOD3 side	No	7 (1706 bp)	3 (545 bp)	0	2 (276 bp)	2527
	CYP19 side	No	6 (942 bp)	3 (1690 bp)	1 (962 bp)	5 (1037 bp)	4631

Ten kilobase intervals with breakpoints (5 kb on either side of the breakpoints) contained 21–73% repetitive elements. Of the breakpoints studied, 3 of 8 were located within repetitive elements.
SINE, short-interspersed transposable element; LINE, long-interspersed transposable element; LTR, long-terminal repeat.

genome and are present in ~1 million copies per haploid genome (27). Long-interspersed nucleotide elements (LINEs) comprise ~20% of the human genome (28) and there are over 500 000 copies in the human genome. The RepeatMasker program showed the region proximal to a breakpoint at MAPK6 side in family 2 was somewhat enriched with DNA repetitive elements (Table 3). Interspersed nucleotide elements, however, were not abundant in the sequences flanking the other breakpoints (Table 3). Thus, interspersed nucleotide elements proximal to breakpoints were also unlikely to be responsible for the inversion mutations observed in individuals or families affected by AES.

As a third possibility, we turned our attention to short, repetitive sequences, which have been shown to be associated with non-homologous recombination through the formation of secondary structures between DNA ends at breakpoints (29). We examined the genomic sequence containing breakpoint junctions. Inversions of inverted repeats, believed to facilitate the formation of 'knot' structures, were detected in both the CGNL1/CYP19 (4/4 matches) (Fig. 7A) and MAPK6/CYP19 (9/12 matches) (Fig. 7B) junctions, suggesting that these rearrangements might be associated with secondary 'knot' structure. Additionally, a direct repeat (8/13 matches) was observed at the TLN2/CYP19 junction (Fig. 7C).

On the basis of these observations, we propose a general model in which loop formations induce intrachromosomal rearrangements giving rise to inversions that permit cryptic transcription of the CYP19 through the CGNL1, MAPK6 and TLN2 promoters (Fig. 7). It appears that sequences with short DNA homology (≥3 nucleotides) were sufficient to cause these rearrangements. Taken together, our data suggest that random heterozygous inversions or deletions can occur at any point within the human genome to create cryptic promoters that drive inappropriate regulation of critical genes.

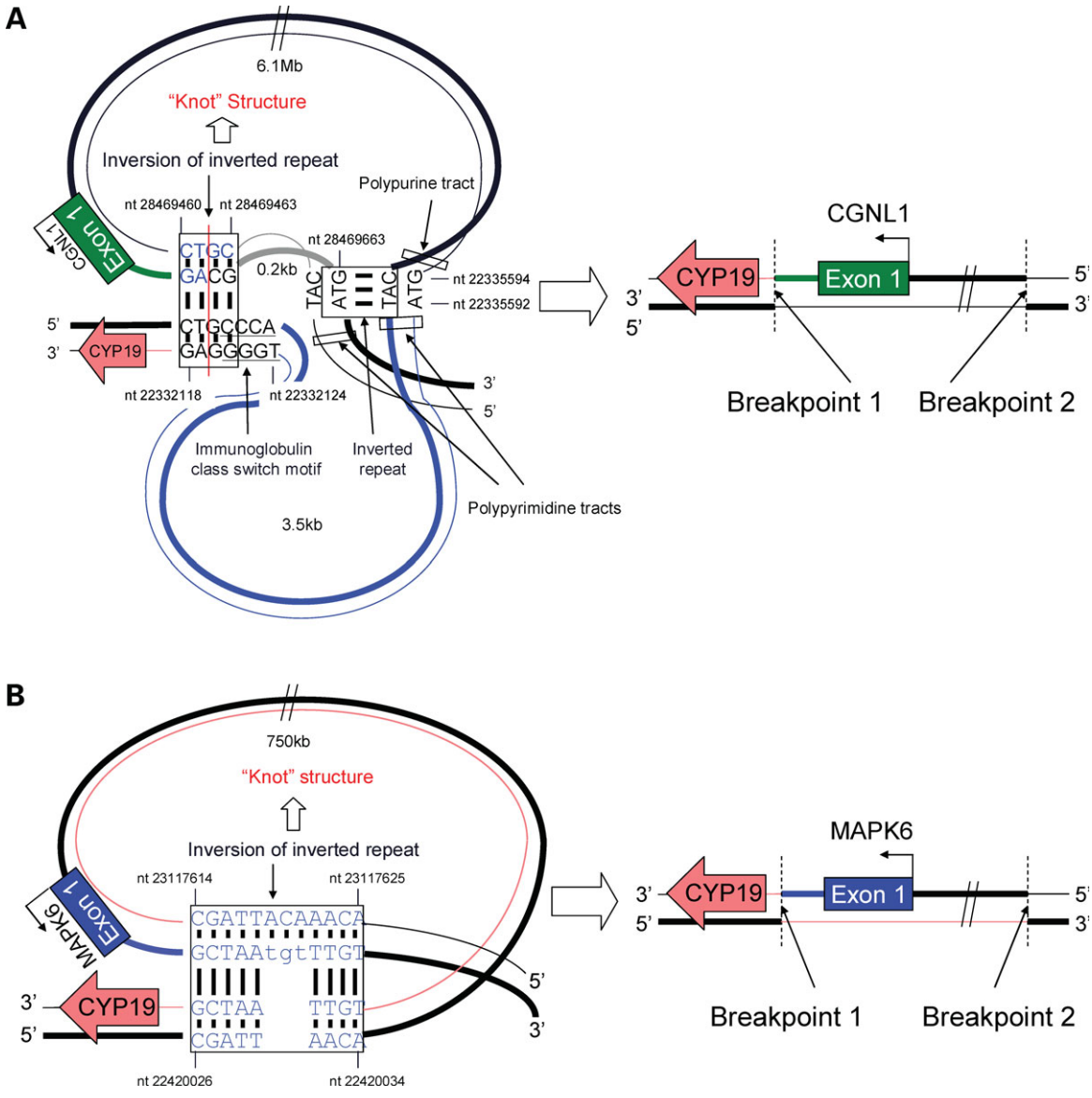

Figure 7. Estimated secondary structures and mutation process. (**A**) CGNL1/CYP19 rearrangement in family 1. A complementary sequence of immunoglobulin class switch (ICS) motif (5′-TGGGG-3′) (38), reported to be over-represented in the translocation breakpoint, was found at breakpoint 1. An inversion of an inverted repeat (29), believed to facilitate the formation of a 'knot' structure, was detected between the surrounding end sequences of the deleted regions of CYP19 (5′-CTgc-3′) and CGNL1 (5′-GAcg-3′). In the vicinity of breakpoint 2, polypyrimidine and polypurine runs flanked the deleted region of the CYP19 gene, whereas polypyrimidine runs existed directly after breakpoint 2 in the CGNL1 gene. Both polypyrimidine and polypurine sequences have been reportedly over-represented in the vicinity of non-homologous recombination (38). From these findings, we propose a mutation process involving inversion probably resulting from secondary loop-formation containing a 'knot structure'. The excision repair of such a secondary loop-structure would result in inversion of the looped 6.1 Mb region with the *CGNL1* gene and looping out the two deleted regions in an ICS-like fashion. (**B**) MAPK6/CYP19 rearrangement in family 2. An inversion of an inverted repeat (9/12 matches) was detected at the breakpoints (29), suggesting a secondary stem loop-induced inversion. (**C**) TLN2/CYP19 rearrangement in sporadic case 2. A direct repeat (8/13 matches) (29), which may cause loop formation was detected at the breakpoints, suggesting a secondary stem loop-induced inversion. Nucleotide numbers correspond to the Contig NT_010194.16.

As in the case of the *CYP19* gene, we now know that physiological promoters as far as 150–200 kb upstream were found to regulate many other genes including the ERα (ESR1) gene that mediates the actions of estrogen (30). We, however, still do not know the exact mechanism of splicing of such extremely long intronic sequences upon the use of far distal promoters.

An animal model of the aromatase excess syndrome has been characterized elegantly in henny-feathered Sebright Bantam roosters (31–33). This chicken strain has an autosomal dominant mutation that has given rise to aromatase overexpression in skin fibroblasts, leading to a female pattern of feather development in roosters (31,33). The demonstration of a novel 5′ untranslated region (5′ UTR) of aromatase mRNA in skin fibroblasts suggested that a cryptic promoter regulated the expression of aromatase (33). It should be noted that a chicken mutation, which persisted >200 years, did not hinder the reproductive capacity of this strain

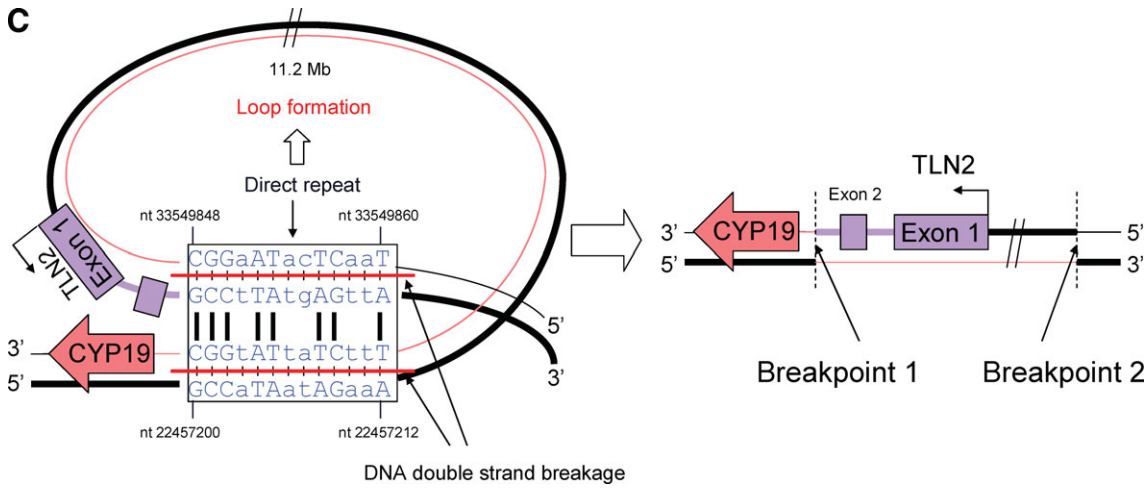

Figure 7. Continued.

(31). The fact that both female and male family members transmitted this mutation in humans suggests that this trait may also be observed in affected humans throughout multiple generations.

It was previously speculated that base pair changes in physiological promoters of the *CYP19* gene may increase the enhancer activity of these regulatory sequences (34). Although this was not demonstrated yet, it remains as another possible mechanism. Nevertheless, we report here a genetic mechanism for systematic overexpression of aromatase, whereby inversions or deletions place constitutively active promoters proximal to the *CYP19* gene. It is possible that subtle chromosomal rearrangements that cause local aromatase overexpression may be common and genetically predispose individuals to the development of various estrogen-dependent pathologies, such as breast and endometrial cancers and endometriosis (35). Furthermore, the mechanism of small chromosomal rearrangements described here may underlie other diseases that involve the dysregulation of critical gene expression.

MATERIALS AND METHODS

Patients

Nine patients (in three unrelated families and two individuals) with AES were enrolled by referral from US and international institutions. All samples were acquired with informed consent in accordance with protocols approved by the human subject protection committees of the respective institutions. Experimental protocols were approved by the institutional review boards of Northwestern University. Family 1 and sporadic case 1 have been described previously (20). Families 2 and 3 have been described elsewhere (19,21). DNA was isolated from peripheral blood cells or LCLs using standard methods. Affected males had prepubertal gynecomastia, early growth, short adult stature and/or hypogonadotropic hypogonadism (19–21). Affected females had premature thelarche, macromastia, irregular uterine bleeding and enlarged uterine size (19). All patients had increased serum estrogen levels (19–21).

Sporadic case 2

Sporadic case 2 was a 36-year-old man who had progressive gynecomastia. He was evaluated at the Pediatric Endocrine Unit at Mass General Hospital for Children. He underwent bilateral mastectomy at age 19. He reached a final height of 182 cm, which was normal for his age and family. Neither his parents nor his relatives had a history of estrogen excess.

Aromatase assay

Aromatase activity was determined by measuring $[^3H]H_2O$ produced upon conversion of [1β-^{3}H]androstenedione to estrone, as reported previously (36). LCLs were cultured in 6-well plates in 20% FBS RPMI1640 for 72 h before adding [1β-^{3}H]androstenedione. The cells were incubated with [1β-^{3}H]androstenedione for 6 h. Incubation was terminated by ice, and medium (2 ml) was transferred into microtubes and centrifuged. The supernatant was subjected to chloroform and charcoal extraction for the removal of all steroids followed by measurement of $[^3H]H_2O$ as previously described (36). The assay was performed in triplicate. Aromatase activity was expressed as the rate of incorporation of tritium into water per milligram protein per 6 h.

Real-time RT-PCR

Messenger RNA was reverse-transcribed from total RNA using Superscript III (Invitrogen, Carlsbad, CA, USA) and random hexamer primers and quantified using real-time PCR. Real-time PCR for the coding region of the *CYP19* gene and GAPDH were carried out using the TaqMan Gene Expression Assay (Applied Biosystems, Foster City, CA, USA). PCR amplification was performed in triplicate employing an ABI PRISM 7900 Sequence Detection System (Applied Biosystems) according to the manufacturer's instructions. cDNA (2 μl) was added to the PCR mixture in a final volume of 20 μl. Thermal conditions for PCR were 50°C for 2 min, 95°C for 10 min and 40 cycles of 95°C for 15 s, 60°C for 1 min.

Rapid amplification of 5′ and 3′ cDNA ends (5′ and 3′ RACE)

To identify the 5′-UTR of the *CYP19* gene, 5′ RACE was performed using the SMART RACE cDNA Amplification Kit (BD Biosciences, Palo Alto, CA, USA), as previously reported (37). Briefly, SMART oligo A-ligated and double-stranded cDNA was synthesized using PowerScript reverse transcriptase (BD Biosciences). The first round of PCR was performed using a universal primer and a 21 bp antisense primer (5′-CAGGAATCTGCCGTGGGAGAT-3′). A nested PCR amplification of the diluted primary PCR mix was performed using a nested universal primer and a 20 bp antisense primer (5′-CAGGCACGATGCTGGTGATG-3′). 3′-RACE was performed in normal skin fibroblasts to characterize the unknown 3′ end of the novel sequence detected in chimeric CYP19 transcripts from sporadic case 2. The amplification reaction was performed using a universal primer and a 22 bp sense primer (5′-AGCTGCTGAGAGG TGGTTTTAT-3′). The resulting PCR products were fractionated on a 1% agarose gel and directly sequenced using the ABI PRISM BigDye Terminator cycle sequencing kit (Applied Biosystems). The sequencing reactions were performed according to the manufacturer's instructions and analyzed on an ABI310 DNA Sequencer (Applied Biosystems).

Amplification and sequencing of inversion junctions

Long-range PCR (LR-PCR) was used to amplify junction breakpoints. A number of forward primers representing sequences 10 kb from the first exons of the identified cryptic promoters and reverse primers representing sequences 10 kb from the CYP19 common exon II were used to generate junction products that were not present in normal control individuals. Primers used to amplify across the junctions by LR-PCR are listed in Table 2. These fragments were gel purified and nested primers were used at one or both ends to generate smaller fragments and sequences across the junction. DNA sequencing was performed using the ABI Prism BigDye v3.1 terminator kit and an ABI 3100 DNA sequencer (Applied Biosystems).

Genomic BAC library for inversion junction clone identification

LR-PCR was unsuccessful for identifying the inversion junction from sporadic case 1. Therefore, a BAC library was constructed from LCL by Bio S&T. PCR-based library screening was performed with the sequence of exon 1 of the *TMOD3* gene. PCR products were visualized on a 1% agarose gel by ethidium bromide staining. Identified BAC clones were cultured overnight in 275 ml of 1 × Luria–Bertani medium containing 5% sucrose and 30 μg/ml chloramphenicol. BAC DNA was extracted using Qiagen Midi Kit (Qiagen, Valencia, CA, USA). BAC end sequences were determined by cycle sequencing with forward (5′-GGATGTGCTGCAAGGCGAT TAAGTTGG-3′) and reverse (5′-CTCTGTATGTTG TGTG GAATTGTGAGC-3′) primers. The sequencing reaction was performed in a 40 μl mixture containing 1 μg of BAC DNA, 16 μl of BigDye (Applied Biosystems) and 0.2 μM of primer under conditions in accordance with the manufacturer's guidelines. PCR products were electrophoresed in an ABI Prism 3100 DNA sequencer and were analyzed by Auto-Assembler (Applied Biosystems). The breakpoint was approached in a walking manner using different primers from either direction. Finally, nested primers were used at both ends to generate smaller fragments to sequence across the junction.

Detection of deleted sequences by real-time PCR

The deleted regions were mapped by a quantitative real-time PCR approach. In order to detect copy number alterations (microdeletions) in family 3, we designed primers for a set of physically mapped amplicons (80–144 bp) covering the 380 kb region between the *DMXL2* and the *CYP19* genes (Table 2). We used samples from the father and son in family 1 as positive controls for a deletion at point A. The average values of normal controls were expressed as 1.0. Thermal conditions for PCR were 50°C for 2 min, 95°C for 10 min and 40 cycles of 95°C for 15 s, and 60°C for 1 min. PCR amplifications were performed in triplicate.

Tissue distribution of gene expression

We determined the expression profile of the five genes by the analysis of expressed sequence tag counts publicly available at the UniGene Web site.

Bioinformatics and sequence analysis

The Blast 2 browser was used for sequence comparisons of the 200 kb 5′ flanking region of the CYP19 gene (nucleotides 22323266–22523265) with the 100 kb regions flanking the CGNL1 (nucleotides 28423266–28523265), TMOD3 (nucleotides 22883266–22983265), DMXL2 (nucleotides 22653266–22753265), MAPK6 (nucleotides 23053266–23153265) and TLN2 (nucleotides 33473266–33573265) genes containing their first exons and breakpoints. Repeat sequence analysis was performed with RepeatMasker 2 for the 10 kb sequences flanking the breakpoints; nucleotides 28464546–28474545 (CGNL1 side) and 22328866–22338865 (CYP19 side) in the CGNL1/CYP19 rearrangement, nucleotides 22918466–22928465 (TMOD3 side) and 22486766–22496765 (CYP19 side) in the TMOD3/CYP19 rearrangement, nucleotides 23112566–23122565 (MAPK6 side) and 22415066–22425065 (CYP19 side) in the MAPK6/CYP19 rearrangement, and nucleotides 33544866–33554865 (TLN2 side) and 22452206–22462205 (CYP19 side) in the TLN2/CYP19 rearrangement. Nucleotide numbers correspond to Contig NT_010194.16.

ACKNOWLEDGEMENTS

This work was supported by grants from the NIH (C67167), AVON Foundation, Lynn Sage Foundation, Northwestern Memorial Foundation and Friends of Prentice (S.E.B.).

Conflict of Interest statement: None declared.

REFERENCES

1. Sebastian, S. and Bulun, S.E. (2001) A highly complex organization of the regulatory region of the human CYP19 (aromatase) gene revealed by the Human Genome Project. *J. Clin. Endocrinol. Metab.*, **86**, 4600–4602.
2. Bulun, S.E., Sebastian, S., Takayama, K., Suzuki, T., Sasano, H. and Shozu, M. (2003) The human CYP19 (aromatase P450) gene: update on physiologic roles and genomic organization of promoters. *J. Steroid. Biochem. Mol. Biol.*, **86**, 219–224.
3. Kamat, A. and Mendelson, C.R. (2001) Identification of the regulatory regions of the human aromatase P450 (CYP19) gene involved in placenta-specific expression. *J. Steroid. Biochem. Mol. Biol.*, **79**, 173–180.
4. Mahendroo, M.S., Mendelson, C.R. and Simpson, E.R. (1993) Tissue-specific and hormonally controlled alternative promoters regulate aromatase cytochrome P450 gene expression in human adipose tissue. *J. Biol. Chem.*, **268**, 19463–19470.
5. Harada, N. (1992) A unique aromatase (P-450AROM) mRNA formed by alternative use of tissue-specific exons 1 in human skin fibroblasts. *Biochem. Biophys. Res. Commun.*, **189**, 1001–1007.
6. MacDonald, P.C., Madden, J.D., Brenner, P.F., Wilson, J.D. and Siiteri, P.K. (1979) Origin of estrogen in normal men and in women with testicular feminization. *J. Clin. Endocrinol. Metab.*, **49**, 905–916.
7. Young, S., Gooneratne, S., Straus, F.H., II, Zeller, W.P., Bulun, S.E. and Rosenthal, I.M. (1995) Feminizing Sertoli cell tumors in boys with Peutz–Jeghers syndrome. *Am. J. Surg. Pathol.*, **19**, 50–58.
8. Coen, P., Kulin, H., Ballantine, T., Zaino, R., Frauenhoffer, E., Boal, D., Inkster, S., Brodie, A. and Santen, R. (1991) An aromatase-producing sex-cord tumor resulting in prepubertal gynecomastia. *N. Engl. J. Med.*, **324**, 317–322.
9. Berensztein, E., Belgorosky, A., de Davila, M.T. and Rivarola, M.A. (1995) Testicular steroid biosynthesis in a boy with a large cell calcifying Sertoli cell tumor producing prepubertal gynecomastia. *Steroids.*, **60**, 220–225.
10. Diamond, F.B., Jr, Root, A.W., Hoover, D.L. and Monteforte, H. (1996) Hetero- and isosexual pseudoprecocity associated with testicular sex-cord tumors in an 8 year-old male. *J. Pediatr. Endocrinol. Metab.*, **9**, 407–414.
11. Bulun, S.E., Rosenthal, I.M., Brodie, A.M., Inkster, S.E., Zeller, W.P., DiGeorge, A.M., Frasier, S.D., Kilgore, M.W. and Simpson, E.R. (1994) Use of tissue-specific promoters in the regulation of aromatase cytochrome P450 gene expression in human testicular and ovarian sex cord tumors, as well as in normal fetal and adult gonads. *J. Clin. Endocrinol. Metab.*, **78**, 1616–1621.
12. Dubois, R.S., Hoffman, W.H., Krishnan, T.H., Rising, J.A., Tolia, V.K., Sy, D.A. and Chang, C.H. (1982) Feminizing sex cord tumor with annular tubules in a boy with Peutz–Jeghers syndrome. *J. Pediatr.*, **101**, 568–571.
13. Lefevre, H., Bouvattier, C., Lahlou, N., Adamsbaum, C., Bougneres, P. and Carel, J.C. (2006) Prepubertal gynecomastia in Peutz–Jeghers syndrome: incomplete penetrance in a familial case and management with an aromatase inhibitor. *Eur. J. Endocrinol.*, **154**, 221–227.
14. Duparc, C., Boissiere-Veverka, G., Lefebvre, H., Laquerriere, A., Vuillermet, P., Landreat, A., Ivell, R., DeRoux, N. and Kuhn, J.M. (2003) An oestrogen-producing seminoma responsible for gynaecomastia. *Horm. Metab. Res.*, **35**, 324–329.
15. Gabrilove, J.L., Sharma, D.C., Wotiz, H.H. and Dorfman, R.I. (1965) Feminizing adrenocortical tumors in the male. A review of 52 cases including a case report. *Medicine (Baltimore).*, **44**, 37–79.
16. Forst, T., Beyer, J., Cordes, U., Pfutzner, A., Kustner, E., Moll, R., Bockisch, A. and Lehnert, H. (1995) Gynaecomastia in a patient with a hCG producing giant cell carcinoma of the lung. Case report. *Exp. Clin. Endocrinol. Diabetes,*, **103**, 28–32.
17. Castro-Magana, M., Angulo, M. and Uy, J. (1993) Male hypogonadism with gynecomastia caused by late-onset deficiency of testicular 17-ketosteroid reductase. *N. Engl. J. Med.*, **328**, 1297–1301.
18. Hemsell, D.L., Edman, C.D., Marks, J.F., Siiteri, P.K. and MacDonald, P.C. (1977) Massive extranglandular aromatization of plasma androstenedione resulting in feminization of a prepubertal boy. *J. Clin. Invest.*, **60**, 455–464.
19. Martin, R.M., Lin, C.J., Nishi, M.Y., Billerbeck, A.E., Latronico, A.C., Russell, D.W. and Mendonca, B.B. (2003) Familial hyperestrogenism in both sexes: clinical, hormonal, and molecular studies of two siblings. *J. Clin. Endocrinol. Metab.*, **88**, 3027–3034.
20. Shozu, M., Sebastian, S., Takayama, K., Hsu, W.T., Schultz, R.A., Neely, K., Bryant, M. and Bulun, S.E. (2003) Estrogen excess associated with novel gain-of-function mutations affecting the aromatase gene. *N. Engl. J. Med.*, **348**, 1855–1865.
21. Hanaki, K., Kinoshita, T., Kawashima, Y., Nagaishi, J., Nishimura, R., Go, A., Ishiguro, K., Tominaga, R. and Kanzaki, S. (2004) Familial gynecomastia associated with increased aromatase expression in skin fibroblasts. In: The Endocrine Society's 86th Annual Meeting ENDO2004, New Orleans, LA, USA.
22. Demura, M., Takeda, Y., Yoneda, T., Furukawa, K., Usukura, M., Itoh, Y. and Mabuchi, H. (2002) Two novel types of contiguous gene deletion of the AVPR2 and ARHGAP4 genes in unrelated Japanese kindreds with nephrogenic diabetes insipidus. *Hum. Mutat.*, **19**, 23–29.
23. Wu, T.C. and Lichten, M. (1994) Meiosis-induced double-strand break sites determined by yeast chromatin structure. *Science,*, **263**, 515–518.
24. Stankiewicz, P. and Lupski, J.R. (2002) Genome architecture, rearrangements and genomic disorders. *Trends Genet.*, **18**, 74–82.
25. Jordan, I.K., Rogozin, I.B., Glazko, G.V. and Koonin, E.V. (2003) Origin of a substantial fraction of human regulatory sequences from transposable elements. *Trends Genet.*, **19**, 68–72.
26. Lander, E.S., Linton, L.M., Birren, B., Nusbaum, C., Zody, M.C., Baldwin, J., Devon, K., Dewar, K., Doyle, M., FitzHugh, W. *et al.* (2001) Initial sequencing and analysis of the human genome. *Nature,*, **409**, 860–921.
27. Weiner, A.M. (2002) SINEs and LINEs: the art of biting the hand that feeds you. *Curr. Opin. Cell. Biol.*, **14**, 343–350.
28. Deininger, P.L., Moran, J.V., Batzer, M.A. and Kazazian, H.H., Jr. (2003) Mobile elements and mammalian genome evolution. *Curr. Opin. Genet. Dev.*, **13**, 651–658.
29. Chuzhanova, N., Abeysinghe, S.S., Krawczak, M. and Cooper, D.N. (2003) Translocation and gross deletion breakpoints in human inherited disease and cancer II: potential involvement of repetitive sequence elements in secondary structure formation between DNA ends. *Hum. Mutat.*, **22**, 245–251.
30. Kos, M., Reid, G., Denger, S. and Gannon, F. (2001) Minireview: genomic organization of the human ERalpha gene promoter region. *Mol. Endocrinol.*, **15**, 2057–2063.
31. George, F.W. and Wilson, J.D. (1980) Pathogenesis of the henny feathering trait in the Sebright bantam chicken. Increased conversion of androgen to estrogen in skin. *J. Clin. Invest.*, **66**, 57–65.
32. McPhaul, M.J., Noble, J.F., Simpson, E.R., Mendelson, C.R. and Wilson, J.D. (1988) The expression of a functional cDNA encoding the chicken cytochrome P-450arom (aromatase) that catalyzes the formation of estrogen from androgen. *J. Biol. Chem.*, **263**, 16358–16363.
33. Matsumine, H., Herbst, M.A., Ou, S.H., Wilson, J.D. and McPhaul, M.J. (1991) Aromatase mRNA in the extragonadal tissues of chickens with the henny-feathering trait is derived from a distinctive promoter structure that contains a segment of a retroviral long terminal repeat. Functional organization of the Sebright, Leghorn, and Campine aromatase genes. *J. Biol. Chem.*, **266**, 19900–19907.
34. Stratakis, C.A., Vottero, A., Brodie, A., Kirschner, L.S., DeAtkine, D., Lu, Q., Yue, W., Mitsiades, C.S., Flor, A.W. and Chrousos, G.P. (1998) The aromatase excess syndrome is associated with feminization of both sexes and autosomal dominant transmission of aberrant P450 aromatase gene transcription. *J. Clin. Endocrinol. Metab.*, **83**, 1348–1357.
35. Bulun, S.E., Lin, Z., Imir, G., Amin, S., Demura, M., Yilmaz, B., Martin, R., Utsunomiya, H., Thung, S., Gurates, B., *et al.* (2005) Regulation of aromatase expression in estrogen-responsive breast and uterine disease: from bench to treatment. *Pharmacol. Rev.*, **57**, 359–383.
36. Ackerman, G.E., Smith, M.E., Mendelson, C.R., MacDonald, P.C. and Simpson, E.R. (1981) Aromatization of androstenedione by human adipose tissue stromal cells in monolayer culture. *J. Clin. Endocrinol. Metab.*, **53**, 412–417.
37. Sebastian, S., Takayama, K., Shozu, M. and Bulun, S.E. (2002) Cloning and characterization of a novel endothelial promoter of the human CYP19 (aromatase P450) gene that is up-regulated in breast cancer tissue. *Mol. Endocrinol.*, **16**, 2243–2254.
38. Abeysinghe, S.S., Chuzhanova, N., Krawczak, M., Ball, E.V. and Cooper, D.N. (2003) Translocation and gross deletion breakpoints in human inherited disease and cancer I: nucleotide composition and recombination-associated motifs. *Hum. Mutat.*, **22**, 229–244.